Inelastic Electron-Proton Scattering at Large Momentum Transfers and the Inelastic Structure Functions of the Proton

G. Miller,* E. D. Bloom, G. Buschhorn,† D. H. Coward, H. DeStaebler, J. Drees,‡ C. L. Jordan, L. W. Mo,§ and R. E. Taylor
Stanford Linear Accelerator Center,‖ Stanford, California 94305

and

J. I. Friedman, G. C. Hartmann,** H. W. Kendall, and R. Verdier
Physics Department and Laboratory for Nuclear Science, Massachusetts Institute of Technology,†† Cambridge, Massachusetts 02139
(Received 2 August 1971; revised manuscript received 8 November 1971)

Differential cross sections for electrons scattered inelastically from hydrogen have been measured at 18°, 26°, and 34°. The range of incident energy was 4.5 to 18 GeV, and the range of four-momentum transfer squared was 1.5 to 21 $(\mathrm{GeV}/c)^2$. With the use of these data in conjunction with previously measured data at 6° and 10°, the contributions from the longitudinal and transverse components of the exchanged photon have been separately determined. The values of the ratio of the photoabsorption cross sections σ_S/σ_T are found to lie in the range 0 to 0.5. The question of scaling of $2M_pW_1$ and νW_2 as a function of ω is discussed, and scaling is verified for a large kinematic range. Also, a new scaling variable which reduces to ω in the Bjorken limit is introduced which extends the scaling region. The behavior of σ_T and σ_S is also discussed as a function of ν and q^2. Various weighted sum rules of νW_2 are evaluated.

I. INTRODUCTION

The measurements we report here extend our earlier study of inelastic electron-proton scattering at forward angles[1] to larger angles (θ), higher four-momentum transfer squared (q^2), and higher electron energy loss (ν), and allow a separation of the two electromagnetic structure functions of the proton. We present the results of the separation with a discussion of the q^2 behavior of these functions and of the implications of the measurements with regard to the question of scaling. The differential cross sections $d^2\sigma/d\Omega\, dE'$ for inelastic electron-proton scattering have been measured at the Stanford Linear Accelerator Center by detecting the scattered electron at laboratory angles of 18°, 26°, and 34°. Measurements were made at incident energies between 4.5 and 18 GeV and at scattered electron momenta between the limit set by elastic scattering kinematics and 2, 1.75, and 1.5 GeV/c, respectively, for the three angles. These measurements have been combined with our earlier measurements at 6° and 10° to provide a separation for various values of q^2 in the range from 1.5 to 11.0 $(\mathrm{GeV}/c)^2$ over a range of W, from 2.0 to 4.0 GeV, where W is the mass of the unobserved hadronic state.

In making the separation we have found it convenient to use the representation for the differential cross section employing the absorption cross sections, σ_T and σ_S, for virtual photons with transverse and longitudinal polarization components, respectively.[2,3] In the limit as $q^2 \to 0$ gauge invariance implies $\sigma_S \to 0$ and $\sigma_T \to \sigma_{\gamma p}$, the latter the total photoabsorption cross section for real photons. On the assumption of one-photon exchange, the differential cross section in the laboratory frame can be written as follows:

$$\frac{d^2\sigma(\theta,E,E')}{d\Omega\, dE'} = \Gamma_T[\sigma_T(q^2,W^2) + \epsilon\sigma_S(q^2,W^2)],$$

$$\Gamma_T = \frac{\alpha}{4\pi^2}\frac{K}{q^2}\frac{E'}{E}\left(\frac{2}{1-\epsilon}\right), \qquad (1)$$

$$\epsilon = \frac{1}{1+2(1+\nu^2/q^2)\tan^2(\frac{1}{2}\theta)}, \quad 0 \le \epsilon \le 1.$$

The quantity $K = (W^2 - M_p^2)/2M_p$, where M_p is the rest mass of the proton, $\nu = E - E'$, and $q^2 = 4EE'\sin^2(\frac{1}{2}\theta)$, where E is the incident electron energy and E' is the scattered energy. The measurements were taken over a large region of q^2-W^2 space as shown in Fig. 1, in order to provide a sufficiently fine grid of data so that the unfolding of radiative effects could be accomplished in a model-insensitive way. Radiatively corrected cross sections at constant values of q^2 and W^2 for different values of ϵ (which correspond to different values of θ) allow the separate determination of σ_T and σ_S, which yields R, defined as σ_S/σ_T.

The differential cross section can also be ex-

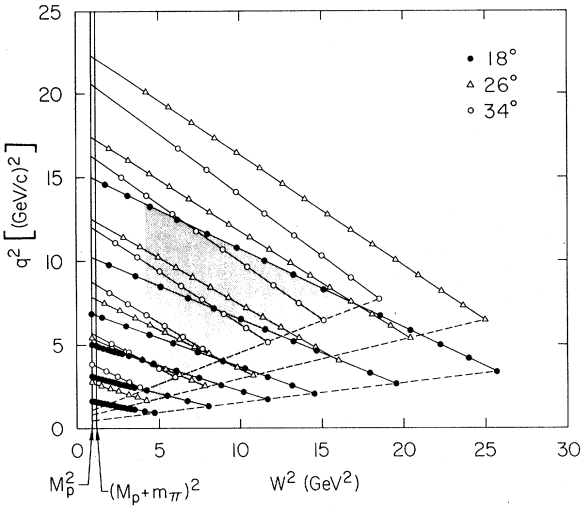

FIG. 1. The regions of the kinematic q^2-W^2 plane covered by the measurements at 18°, 26°, and 34°. The symbols show where cross sections were measured. The shaded area in this figure and the area marked "Separation Region" in Fig. 4 represent the region where data at three or more angles exist. Previously measured 6° and 10° data were also used in the separations.

pressed in terms of two structure functions W_1 and W_2 (Ref. 3) such that

$$\frac{d^2\sigma}{d\Omega dE'} = \frac{4\alpha^2(E')^2}{q^4}\left[W_2(q^2,W^2)\cos^2(\tfrac{1}{2}\theta) + 2W_1(q^2,W^2)\sin^2(\tfrac{1}{2}\theta)\right]. \quad (2)$$

These structure functions are related to the two absorption cross sections for virtual photons in the following way:

$$W_2 = \frac{K}{4\pi^2\alpha}\left(\frac{q^2}{q^2+\nu^2}\right)(\sigma_T+\sigma_S), \qquad W_1 = \frac{K}{4\pi^2\alpha}\sigma_T. \quad (3)$$

Thus the structure functions W_1 and W_2 may be found directly from the values of σ_T and σ_S from the separation procedure.

II. EXPERIMENTAL METHOD

The experimental equipment and techniques used in this experiment were very similar to those used in an experiment in which the elastic form factors of the proton were measured to large q^2.[4] Thus the emphasis here will be placed on problems specific to this experiment and on modifications to the apparatus based in part on the experience gained during the past several years, since the elastic scattering measurements, with the SLAC spectrometer facility. The incident electron beam, varying in energy between 4.5 and 18 GeV, was typically momentum-analyzed to $\Delta p/p = \pm 0.5\%$ and was focused at the target to a spot approximately 3 mm high and 6 mm wide. The uncertainty in the absolute energy of the beam was ±0.2% independent of energy. The incident-beam position and angle, monitored continuously throughout the experiment with two retractable zinc sulphide screens located upstream and a fixed screen located just downstream of the hydrogen target, remained constant both horizontally and vertically to ±1 mm and ±0.1 mrad, respectively. The number of incident electrons was measured to an absolute accuracy of ±0.5% by two toroidal beam monitors which were intercalibrated with a Faraday cup several times during the experiment. No energy dependence of the monitor calibration was observed to this level of accuracy. Collimation studies of the incident beam were made to eliminate the possibility of a low-energy, large-area beam halo which could introduce systematic errors in the data taken at low secondary momenta.

The liquid-hydrogen target was specially designed to accommodate the very large beam intensities used in this experiment.[5] These intensities were as high as 50 mA, in a 1.6-μsec beam pulse. Beam repetition rates up to 360 times per second were employed. The condensing target contained a pump which recirculated the liquid hydrogen in a closed loop from the target cell through a heat exchanger in contact with a liquid-hydrogen reservoir. Extensive tests showed that the recirculation eliminated variations of target density with variations of electron-beam cross-sectional area and intensity, to an accuracy of 2% in the scattering cross section. In addition, the density was shown to be constant within ±1% throughout the actual experiment by detecting with the SLAC 1.6-GeV/c spectrometer protons recoiling elastically from the target. The density of the liquid hydrogen was 0.070 g/cm^3, determined from the temperature of the hydrogen measured by two hydrogen vapor-pressure thermometers inserted in the target above and below the beam line. The 7-cm-diameter target cell was an aluminum cylinder with 0.003-in.-thick walls. The wall contribution to the scattering was measured by using an identical, but empty, aluminum cylinder mounted directly below the target assembly. Scattering from the replica target and other windows was typically 10% of the full target rate.

The scattered particles were momentum-analyzed by the SLAC 8-GeV spectrometer.[4] The spectrometer focused point-to-point and dispersed momentum in the vertical plane, and focused line-to-point and dispersed the horizontal scattering angle in the horizontal plane. The momentum dispersion was approximately 3 cm per percent and the horizontal projected angle dispersion was ap-

proximately 4.5 cm per milliradian. The magnets were calibrated to the same standard shunt as the magnets defining the incident beam energy. The alignments of the magnetic elements were frequently monitored during the experiment. All observed misalignments were such as to change a ray by less than one fifth of the designed resolution.

An attempt was made during this experiment to understand and reduce the uncertainty in the solid-angle acceptance of the spectrometer which had been used in the previous elastic scattering experiments.[4] As described in Ref. 4, a computer model of the spectrometer has been derived which satisfactorily reproduced the optics measurements obtained by directing the incident beam into the spectrometer and mapping out the acceptance with a large family of rays of various energies and angles. Based on this model, lead apertures, each several radiation lengths thick, were installed in the spectrometer to define more sharply the acceptance and to simplify the acceptance calculations. The vertical projected angular acceptance, approximately 60 mrad, was defined by a lead aperture located before the last quadrupole magnet. The total acceptance of the spectrometer $\Delta\Omega(\Delta p/p)$ was 25.4 mrad^2. This was calculated analytically and by a Monte Carlo method. The calculations agreed to ±1%.

Particle detection, identification, and angle-momentum measurements were accomplished by a system of detectors consisting in sequence of a threshold gas Čerenkov counter (C), a large trigger counter consisting of five overlapping plastic scintillation counters, a scintillation-counter hodoscope of 55 vertical elements to measure particle scattering angles, a scintillation-counter hodoscope of 41 horizontal elements to measure particle momenta, another large trigger counter identical to the first, a telescope of three scintillation counters preceded by one radiation length of lead (DEX), and a total absorption, lead-Lucite shower counter (TA). The hodoscope and trigger counters were the same as those used in the elastic electron scattering experiment of Kirk *et al.*[4]

The two orthogonal hodoscopes defined the resolution of the spectrometer to ±0.05% in momentum and ±0.15 mrad in horizontal scattering angle. A restricted set of these hodoscope counters was used to define a smaller acceptance to investigate possible effects due to scattering from the lead that masked the hodoscopes. Average cross sections calculated with the total acceptance and with the restricted acceptance agreed to ±1% in the case where the cross sections were not strongly varying with momentum. The calculations of the acceptance were considered accurate to ±2%. Further details on the spectrometer and the acceptance calculations may be found in Ref. 6.

After each event, an on-line computer system, utilizing an SDS 9300 computer, scanned the hodoscope buffers, the charge monitors, and six analog-to-digital converters. This information was written on magnetic tape for later analysis. A continuously updated cross section as well as updated detector efficiencies and inefficiencies due to hodoscope multiple tracks were evaluated on line using a fraction of the events written on tape. The largest instantaneous counting rates occurred in the large trigger counters and were kept less than 5 per machine pulse by regulating the incident-beam intensity. The fast electronic dead-time effects were less than 3%. The number of events per pulse was kept at a rate less than 0.3 events per pulse.

III. DATA ANALYSIS

The electron yields and cross sections for a particular E, E', θ setting, target type, and spectrometer polarity were calculated by counting the number of events on the data tape satisfying three different requirements, allowing successively greater electron-pion discrimination. The discrimination requirements were (a) a large pulse height from the TA counter corresponding to a 99% efficiency for a pure electron sample; (b) a signal from the Čerenkov counter plus requirement (a); and (c) large pulse heights from all three DEX scintillation counters plus condition (b). Where the three cross sections agreed within statistics the least restrictive requirement having the largest number of successful events was used. All events were required to have good signals from both trigger scintillation counters and to represent particles unambiguously passing through the restricted set of hodoscope counters.

Discrimination of electrons from pions became a problem at the lowest secondary energies. The largest pion-to-electron ratio encountered was about 300:1 where the pion rejection of the combined system (C DEX TA) was about 2×10^4:1, and the electron efficiency was 0.74. This low efficiency was due to the DEX system which had an energy-dependent efficiency for electrons that ranged from 0.74 at 2 GeV to 0.88 at 8 GeV and had an uncertainty of ±1.5%. For most points, DEX was not used, and the electron efficiency was 0.97. The largest correction for residual pion contamination was 4%; generally it was less than 1%.

Corrections were made for the electron detection efficiency of all counters, for the computer logging deadtime (less than 15%), and for ambiguous hodoscope bit patterns (typically 7%). The final mea-

sured cross section was corrected by subtracting the cross section for electrons scattered from the target walls and the contribution from electrons coming from π^0 decay and pair production. This contribution was measured by reversing the polarity of the spectrometer and was negligible over most of the spectra except at the lowest scattered energies where it was always less than 25%.

The measured cross sections were corrected for radiative effects using the formulas in the Appendix. We here describe the procedure in a qualitative way. First, the elastic radiative tail was subtracted. This was calculated using the formula of Tsai[7] for electron bremsstrahlung during the elastic scattering which is exact to lowest order in α. Radiative-energy degradation of the incident and final electrons by the surrounding target material was also included along with corrections for multiple-photon effects and radiation from the recoiling proton. After the subtraction of the elastic tail, the inelastic radiative effects were removed in an unfolding procedure using a peaking-factorization approximation which allowed the radiative tail to be expressed as the sum of two one-dimensional integrals involving the previously corrected cross sections at the same angle. The particular version of the peaking-factorization approximation used was determined by a direct comparison with an exact calculation of the inelastic radiative tail, assuming a model which approximated the experimentally determined inelastic form factors.

The inelastic radiative-tail corrections were assigned an error of ±10% of the correction to take into account both the inaccuracy of the peaking approximation and errors introduced by interpolation of the cross section. The different methods of interpolation used changed the corrected cross sections by less than half of the statistical error. The elastic tail corrections were assigned an average error of ±3% of the correction which reflects uncertainties as large as 5%. The maximum total radiative correction was 30%, and the corrections were generally smaller than those at the lower angles.[1]

Elastic electron-proton scattering was measured for nine combinations of incident energy and scattering angle. These data were taken for two reasons: (1) comparison of these data with the elastic data taken earlier at SLAC[4] provided a check of the over-all normalization of this experiment; (2) comparison of these data with those taken earlier at 6° and 10° with the 20-GeV spectrometer[1] provided an inter-spectrometer normalization check so that the two sets of inelastic data could be used together to determine separately the two structure functions.

Two different analyses of the elastic data were carried out. In the first, cross sections were corrected for the effects of radiation using an unfolding method described in Ref. 4. In the second, the

TABLE I. The principal sources of uncertainty in the final cross sections, excluding counting statistics, are summarized in this table. The uncertainties with point-to-point variation were combined in quadrature with the counting statistics (with the exception of the DEX uncertainty, as noted) to arrive at the cross-section errors given in Table II. These are our estimates of the standard deviations. An over-all normalization uncertainty, which we take to be ±5%, is not included in Tables II or III.

	Point-to-point variation (%)	Over-all normalization uncertainties (%)
Energy and angle of incident beam	0	±0.5
Charge monitor	±0.3	±0.5
Target thickness (g/cm^2)	±1	±2
Spectrometer acceptance	±1	±2
Counter efficiencies		
TA	0	±0.5
Čerenkov [a]	0	±1
DEX [a]	±1.5 [b]	±1.5
Electronic deadtimes	<±1	0
Pion contamination	≤±2	0
Radiative correction		
Elastic tail	±3% of correction	0
Continuum	±10% of correction	0

[a] The uncertainty appropriate to this counter is only relevant to those runs where the counter was employed in the analysis.

[b] This contribution was added linearly after the others had been combined in quadrature.

theoretical cross section was folded with radiation effects, the incident energy spectrum, and the spectrometer resolution using the elastic form factors previously reported by the MIT-SLAC collaboration[8] together with the elastic scattering measurements taken at 6° and 10° with the 20-GeV spectrometer. These predictions were then compared with the measurements. Both methods gave similar results, indicating that any relative systematic errors between the present apparatus and the 20-GeV spectrometer are not apparent compared with the statistical errors of approximately 3%. This result is especially important for those separations of σ_T and σ_S that also rely on data taken at small angles with the 20-GeV spectrometer. Typically, a systematic 3% difference between the 6° and 10° data and the present data would change the ratio $R=\sigma_S/\sigma_T$ by 0.06. This uncertainty is small compared to the statistical errors in the values of R.

Table I contains a summary of the estimates of various uncertainties.

Figure 2 shows the radiatively corrected spectrum for $E=18$ GeV, and $\theta=26°$, along with the radiative correction factor, defined as the ratio of the final corrected cross section to the measured cross section.

IV. RESULTS

Table II gives the values of the radiatively corrected cross sections for which $W \geq 1.8$ GeV. The quoted errors reflect both counting statistics and the parts of other estimated uncertainties that have point-to-point variation, two of which are the errors described above for the elastic and inelastic radiative tails. Not included is an additional overall systematic error that is estimated to be ±5%.

The shaded area of the q^2-W^2 plane in Fig. 1 shows the kinematic range over which σ_S and σ_T can be separated requiring data at a minimum of three values of ϵ (i.e., using the data taken at 6°, 10°, 18°, 26°, and 34°). Actual data points at different angles for the same values of q^2 and W^2 exist only for $q^2=4$ (GeV/c)^2; $W=2$, 3, and 4 GeV. However, the data at each angle are sufficiently finely spaced that they can be reliably interpolated to a particular point in the q^2-W^2 plane. Separations with several different interpolation methods indicated that the results were insensitive to the particular procedure used. Interpolations at twenty points (q^2, W^2) were chosen to represent the actual amount of data taken within the shaded area of Fig. 1, some emphasis being placed on those areas with data at four or five values of ϵ. Figure 3 shows four examples of ϵ plots used to obtain these ratios. The assumption of one-photon exchange,

TABLE II. Radiatively corrected differential cross sections for inelastic electron-proton scattering. All measured points with $W \geq 1.8$ GeV are listed. The errors are approximately statistical standard deviations. An estimated over-all systematic error of ±5% is not included.

θ (deg)	E (GeV)	E' (GeV)	$d^2\sigma/d\Omega dE'$ (10^{-35} cm^2/sr GeV)
18	4.501	2.250	7600 ±430
		2.000	7000 ±450
	6.503	3.500	1879 ± 54
		3.000	2413 ± 75
		2.500	2593 ± 93
		2.000	2510 ±120
	8.598	4.780	460 ± 15
		4.500	572 ± 17
		4.000	779 ± 44
		3.500	957 ± 36
		3.000	1036 ± 50
		2.500	1229 ± 65
		2.000	1330 ±130
	10.404	5.500	180.6 ± 6.3
		5.000	284 ± 10
		4.500	409 ± 16
		3.940	512 ± 23
		3.500	604 ± 32
		3.000	630 ± 40
		2.500	751 ± 47
		2.000	801 ± 99
	13.299	7.000	19.88 ± 0.90
		6.500	49.2 ± 1.9
		6.000	93.0 ± 3.6
		5.500	135.8 ± 5.6
		5.000	178.2 ± 7.7
		4.500	208 ± 15
		4.000	263 ± 21
		3.500	306 ± 28
		3.090	315 ± 23
		2.500	417 ± 49
		2.000	533 ± 74
	17.000	8.000	7.08 ± 0.35
		7.500	15.17 ± 0.56
		7.000	29.9 ± 1.1
		6.500	44.8 ± 1.7
		6.000	64.3 ± 2.6
		5.500	86.9 ± 3.4
		5.000	101.1 ± 7.4
		4.500	122.8 ± 9.4
		4.000	145 ± 12
		3.500	173 ± 16
		3.000	191 ± 20
		2.500	239 ± 31
		2.000	271 ± 54
26	4.494	2.000	1410 ± 67
		1.800	1518 ± 81

TABLE II *(Continued)*

θ (deg)	E (GeV)	E' (GeV)	$d^2\sigma/d\Omega dE'$ (10^{-35} cm^2/sr GeV)	θ (deg)	E (GeV)	E' (GeV)	$d^2\sigma/d\Omega dE'$ (10^{-35} cm^2/sr GeV)
26	6.700	2.940	212.6 ± 7.8	26	18.030	3.750	12.9 ± 1.2
		2.750	283.1 ± 10			3.500	15.3 ± 1.7
		2.500	340 ± 14			3.250	21.5 ± 1.7
		2.250	407 ± 19			3.000	25.7 ± 2.5
		2.000	504 ± 25			2.750	32.9 ± 4.1
		1.750	585 ± 51			2.500	39.4 ± 5.2
	8.696	3.750	32.2 ± 2.0			2.250	45.7 ± 7.3
		3.500	57.2 ± 3.0			2.000	56 ± 10
		3.250	91.7 ± 3.7			1.750	81 ± 16
		3.000	119.9 ± 5.0	34	4.501	1.600	404 ± 22
		2.750	154.9 ± 6.8			1.400	533 ± 31
		2.500	195.5 ± 9.7			1.200	652 ± 41
		2.270	229 ± 12		5.795	2.020	108.0 ± 7.6
		2.000	275 ± 17			1.750	175.3 ± 9.6
		1.750	317 ± 20			1.500	252 ± 21
	11.905	4.500	4.70 ± 0.48			1.250	356 ± 33
		4.250	9.34 ± 0.99		7.899	2.500	24.8 ± 1.6
		4.000	17.7 ± 1.0			2.250	38.2 ± 3.3
		3.750	25.9 ± 1.6			2.000	62.4 ± 5.1
		3.500	35.1 ± 2.2			1.750	90.4 ± 8.0
		3.250	47.0 ± 4.5			1.480	125 ± 12
		3.000	63.4 ± 6.2			1.250	153 ± 21
		2.750	76.9 ± 7.7				
		2.500	91.2 ± 9.9		9.999	3.000	3.02 ± 0.35
		2.250	113 ± 12			2.750	8.60 ± 0.57
		2.000	121 ± 17			2.500	15.03 ± 0.86
		1.670	161 ± 23			2.250	26.1 ± 1.2
						2.000	36.4 ± 2.9
	15.006	5.000	1.34 ± 0.17			1.750	47.2 ± 4.4
		4.750	2.87 ± 0.26			1.500	70.3 ± 7.4
		4.500	5.55 ± 0.39			1.250	104 ± 13
		4.250	8.07 ± 0.50				
		4.000	13.83 ± 0.91		12.500	3.250	1.22 ± 0.19
		3.750	18.4 ± 1.5			3.000	3.52 ± 0.40
		3.500	23.3 ± 1.3			2.750	7.57 ± 0.55
		3.250	31.6 ± 1.8			2.500	10.32 ± 0.64
		3.000	39.6 ± 2.3			2.250	17.1 ± 1.7
		2.750	45.9 ± 4.3			2.000	21.9 ± 2.4
		2.500	52.0 ± 5.4			1.750	32.1 ± 4.0
		2.250	62.7 ± 7.6			1.500	47.8 ± 6.6
		2.000	76 ± 10			1.250	61 ± 13
		1.750	79 ± 15				
					14.996	3.250	0.85 ± 0.25
	18.030	5.500	0.500 ± 0.090			3.000	2.29 ± 0.38
		5.250	1.09 ± 0.15			2.750	4.30 ± 0.53
		5.000	1.31 ± 0.20			2.500	7.21 ± 0.99
		4.750	2.76 ± 0.29			2.250	11.8 ± 1.8
		4.500	4.78 ± 0.39			2.000	16.7 ± 2.0
		4.250	7.66 ± 0.55			1.750	19.6 ± 3.0
		4.000	10.14 ± 0.99			1.500	32.6 ± 5.4

which underlies the definition of the electromagnetic structure functions, implies a linear dependence of $(d^2\sigma/d\Omega dE')/\Gamma_T$ on ϵ for a particular point (q^2, W^2). The data are everywhere consistent with this requirement.

Table III gives the 23 values of R, σ_T, σ_S, W_1, and W_2 along with their estimated random errors, using the data taken at 6°, 10°, 18°, 26°, and 34°. The errors in R take account of the correlation between σ_S and σ_T. The R values are in the range 0 to 0.5, and no striking kinematic variation is apparent. In addition to the random errors quoted, we estimate that there are systematic errors that might change the values of R by ±0.06.

On the assumption that R is a constant in this kinematic range, we find that for this particular set of points the average value of $R = 0.18 \pm 0.10$, where the above-mentioned systematic error is included linearly. The values of R obtained are also compatible with $R = 0.031(q^2/M_p^2)$ and with $R \approx q^2/\nu^2$. These two forms are suggested by theoretical considerations.[9] Undoubtedly, various other forms would also be compatible with our results.

V. DISCUSSION

From the results of the experiment at 6° and 10° (Ref. 1) combined with the assumption of a predominantly transverse electromagnetic interaction (that is, the ratio $\sigma_S/\sigma_T = R$ is small) it was found that νW_2 depended only on the ratio of q^2 and ν over a substantial range of the data.[10] This property is called "scaling" in the variable $\omega \equiv 2M_p\nu/q^2$. Bjorken had predicted the possibility of this behavior in the asymptotic kinematic region reached by letting q^2 and ν go to infinity with ω held constant.[11] Our measured values of R support the earlier assumption that led to scaling of the 6° and 10° data. Now we discuss the validity of scaling behavior in the light of these experimental determinations of R and, additionally, over a wider range of q^2 covered by the large-angle data. In Fig. 4 the shaded area labeled "Separation Region" contains the kinematic locations of the points available for the separation studies. Within this region, W_1 and W_2 may be separately determined without any assumption about the relative contributions from the transverse and longitudinal components of the cross sections. To investigate possible scaling behavior elsewhere in the full kinematic region of our data including the data at 6° and 10°, bounded by the heavy line in Fig. 4, values of R have been obtained by *extrapolation* of the measured values. In order to determine the sensitivity of our knowledge of νW_2 to variations in the method of extrapolation, we have employed the three parametrizations of R (see Sec. IV), all consistent with the measured values. It has been found that the conclusions reported below concerning scaling behavior are insensitive to the choice among these forms.

Throughout the remainder of this paper a constant value of $R = 0.18$ has been assumed over the full kinematic region of measurement. With this assumption, each cross section yields values for W_1 and W_2. To test for scaling behavior it is useful to plot νW_2 for fixed ω as a function of q^2, or equivalently, as a function of W, the mass of the unobserved, final hadronic state. [W, q^2, and ω are related by $W^2 = 2M_p\nu + M_p^2 - q^2 = q^2(\omega - 1) + M_p^2$.] For constant ω, scaling behavior is exhibited in such a plot if νW_2 is independent of W (or q^2). Values of νW_2 are shown in Fig. 5, calculated from interpolations of radiatively corrected spectra measured at 6°, 10°, 18°, 26°, and 34° (i.e., interpolations over the full kinematic region of Fig. 4). The plots are presented for representative values of ω; $\omega = 1.5$, 2, 3, 6, and 12. Scaling behavior is not expected where there are observable resonance "bumps" because resonances occur at fixed W, not at fixed ω, nor can it occur for $q^2 \to 0$, because νW_2 cannot depend solely on ω in this limit. By inspecting the plots in Fig. 5 and other similar graphs we have come to a number of conclusions regarding the validity of scaling in several kinematic regions. These conclusions are summarized below; the regions, with the kinematic variables, are shown in Fig. 4.

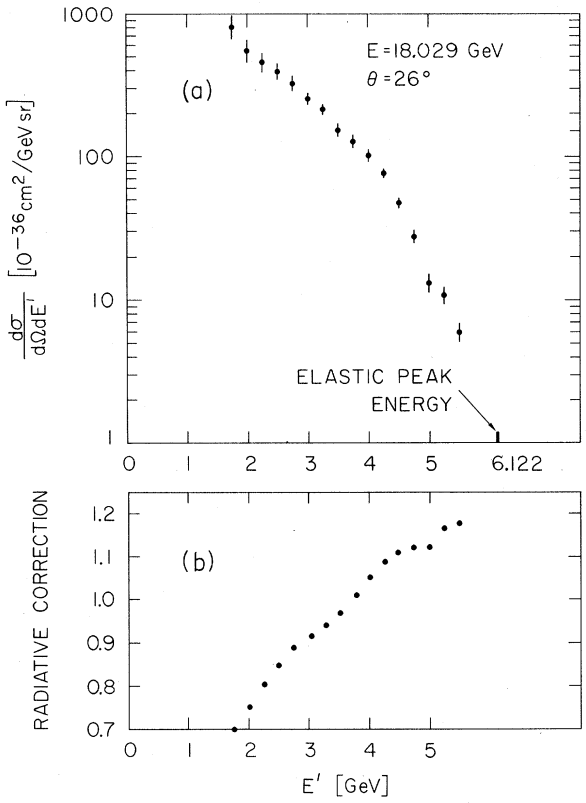

FIG. 2. (a) The radiatively corrected inelastic scattering spectrum $d^2\sigma/d\Omega dE'$ for $E = 18$ GeV, $\theta = 26°$. (b) The radiative correction applied to the data as a function of E', defined as the ratio of the final corrected cross section to the measured cross section.

1. For 4 < ω < 12 (Region B)

For $W > 2.0$ GeV and $q^2 > 1.0$ (GeV/c)^2, νW_2 is a constant within experimental errors and hence "scales" in ω (or, indeed, in any other variable). The range of kinematics for the measurements included in this test covers q^2 from 1 to 7 (GeV/c)^2

TABLE III. R, σ_T, σ_S, W_1 and W_2 for 23 values of q^2 and W^2 using data taken at 6°, 10°, 18°, 26°, and 34°. The errors arise from the propagation of the errors given in Table II. The effects of over-all systematic errors are not included. We estimate that systematic errors could make R uncertain by about ±0.06.

q^2 [(GeV/c)^2]	W (GeV)	σ_T (10^{-30} cm^2)	σ_S (10^{-30} cm^2)	R	$2M_pW_1$	νW_2
1.5	2.0	42.8 ±5.3	−2.8 ±6.6	−0.06±0.15	1.19 ±0.15	0.290±0.012
1.5	2.5	31.7 ±3.3	4.8 ±3.7	0.15±0.13	1.52 ±0.16	0.344±0.005
1.5	3.0	26.7 ±2.8	5.4 ±3.3	0.20±0.14	1.93±0.20	0.343±0.007
1.5	3.3	25.3 ±2.8	5.8 ±3.6	0.23±0.17	2.26 ±0.25	0.347±0.011
3.0	2.0	16.1 ±1.9	0.75±2.6	0.05±0.17	0.45 ±0.05	0.179±0.009
3.0	2.5	15.8 ±1.5	2.0 ±2.0	0.12±0.14	0.76 ±0.07	0.265±0.008
3.0	3.0	15.7 ±1.6	1.7 ±2.2	0.11±0.15	1.14 ±0.11	0.314±0.014
3.0	3.4	13.3 ±2.0	4.3 ±2.8	0.32±0.26	1.27 ±0.19	0.349±0.019
4.0	2.0	8.8 ±1.3	2.0 ±1.7	0.23±0.23	0.244±0.038	0.131±0.005
4.0	3.0	11.0±1.2	2.0 ±1.8	0.18±0.18	0.799±0.086	0.284±0.016
4.0	4.0	9.0±1.7	4.5 ±3.0	0.50±0.43	1.22 ±0.23	0.369±0.039
5.0	2.0	5.82±0.63	1.0 ±0.9	0.17±0.17	0.162±0.018	0.092±0.004
5.0	2.5	7.38±0.57	1.1 ±0.8	0.15±0.12	0.353±0.027	0.169±0.005
5.0	3.0	8.23±0.65	1.4 ±1.0	0.17±0.13	0.596±0.047	0.240±0.009
5.0	3.4	8.0 ±1.2	2.2 ±1.8	0.27±0.27	0.763±0.113	0.289±0.019
8.0	2.0	1.82±0.25	0.58±0.35	0.32±0.24	0.051±0.007	0.039±0.002
8.0	2.5	2.95±0.27	0.57±0.41	0.20±0.16	0.141±0.013	0.087±0.004
8.0	3.0	3.55±0.33	1.30±0.59	0.37±0.20	0.257±0.024	0.157±0.009
8.0	3.5	4.15±0.54	1.6 ±1.1	0.39±0.30	0.420±0.055	0.224±0.021
8.0	4.0	4.99±0.74	0.3 ±1.8	0.06±0.37	0.67 ±0.10	0.235±0.048
11.0	2.0	0.74±0.16	0.34±0.23	0.46±0.40	0.021±0.004	0.020±0.001
11.0	2.5	1.44±0.18	0.28±0.28	0.20±0.22	0.069±0.008	0.048±0.003
11.0	3.0	1.82±0.22	0.89±0.41	0.49±0.29	0.132±0.016	0.102±0.008

and values of W between 2 and 5 GeV.

2. For $\omega < 4$ (Region A)

In this region of ω the number of measurements of νW_2 above the resonance region is considerably increased by the large-angle data. The experimental values of νW_2 scale for $W > 2.6$ GeV, but νW_2 appears to increase as W decreases below 2.6 GeV. This region covers kinematic ranges of W between 2.6 and 4.9 GeV, and of q^2 between 2 and 20 (GeV/c)^2.

3. For $\omega > 12$ (Region C)

There are relatively few points above $q^2 = 1$ (GeV/c)^2 and no points above $q^2 = 2$ (GeV/c)^2, making it difficult to determine any variation of νW_2 with changing q^2. There are no measurements of R in this region, and the values of νW_2 are especially sensitive to variations in R. The large-angle data have a maximum ω of 8 and influence the values of νW_2 for $\omega > 12$ only through the values of R determined in the low-ω region. Scaling cannot be tested critically in this region, since the uncertainty in R prevents the large-ω behavior of νW_2 from being known with assurance. If $R = 0.18$ is assumed, then for $q^2 > 0.8$ (GeV/c)^2 νW_2 decreases slightly as ω increases. However, for larger values of R, consistent with the extrapolated values, νW_2 is constant. Preliminary analysis of more recent data does not resolve these questions.[12]

These conclusions, based on data which extend the q^2 range of previous νW_2 measurements and

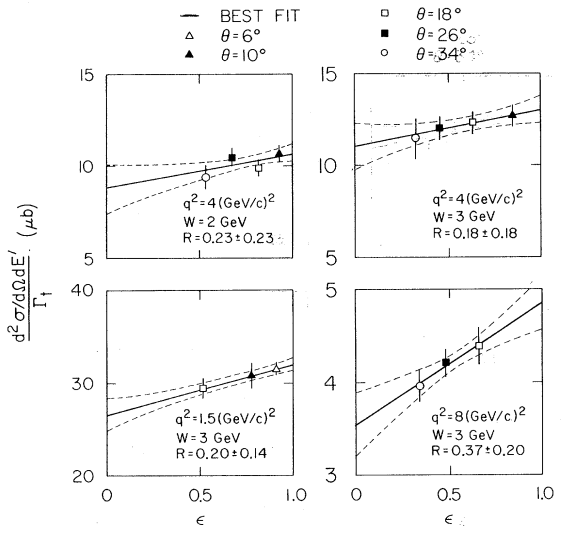

FIG. 3. Typical examples illustrating the separate determination of σ_S and σ_T. The straight solid lines are best fits to Eq. (1). The dashed lines indicate the one-standard-deviation values of the fits. The assumption of one-photon exchange made in calculating σ_S and σ_T implies that linear fits should be satisfactory. For the two upper graphs measured data exist at each angle. For the two lower graphs the data were interpolated. Effects of over-all systematic errors are not included.

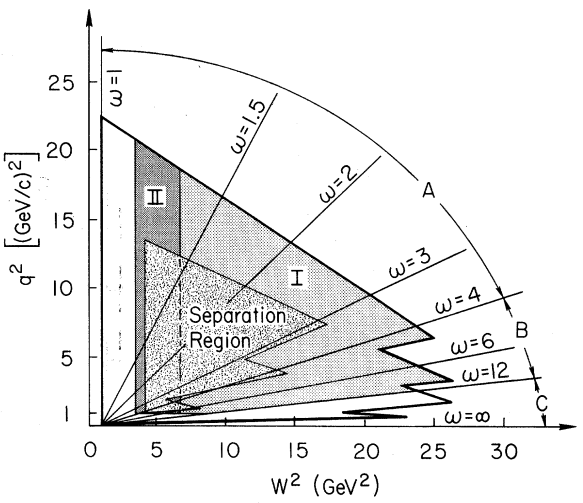

FIG. 4. The kinematic plane in q^2 and W^2 is shown along with lines of constant ω, the scaling variable $2M_p\nu/q^2$. The heavy line bounds all data points measured at 6°, 10°, 18°, 26°, and 34°. The region marked "Separation Region" includes all points where data at three or more angles exist. Various values of ω are indicated with $\omega=\infty$ coinciding with the $q^2=0$ abscissa and $\omega=1$ corresponding to elastic scattering ($W^2=0.88$ GeV^2). Region I indicates the region where the data are consistent with scaling in $\omega=2M\nu_p/q^2$. Region II indicates the extension of the scaling region if the data are plotted against $\omega'=1+W^2/q^2$. The ranges A, B, and C in the variable ω indicated in the figure are discussed in the text.

which include measurements of R, confirm the scaling behavior of νW_2 as a function of ω for $q^2>1$ (GeV/c)^2 as indicated by the earlier 6° and 10° data. Though these studies cover an extensive kinematic region, we would, however, give greater emphasis to conclusions based on data from the separation region in Fig. 4 where the analysis relies on interpolations between measured values of R.

As a byproduct of studying the behavior of the large-angle data at small ω we discovered that for the whole range of ω the scaling region is extended from $W\approx 2.6$ GeV down to $W\approx 1.8$ GeV (which is approaching a resonance bump) if a new variable $\omega'\equiv\omega+a/q^2$ is used instead of ω. The constant a was determined to be 0.95 ± 0.07 (GeV/c)^2 by fitting the data with $W>1.8$ GeV and $q^2>1$ (GeV/c)^2.[13] The quoted error on a was derived from the covariance matrix of the fit and does not include systematic errors or any contribution from the uncertainty in R. The statistical significance of a being different from zero is greatly reduced in a fit to the data for $W>2.6$ GeV, implying that functions of either ω or ω' give satisfactory statistical fits to the data in this kinematic range. In what follows we use $a=M_p^2=0.88$ (GeV/c)^2, which gives $\omega'=\omega+M_p^2/q^2=1+W^2/q^2$. Regarding ω' we note that (a) in the Bjorken limit ω' becomes equal to ω so the two variables have the same asymptotic properties, and (b) in the kinematic region covered by our measurements, q^2 and ν may not be large in the sense of the Bjorken limit and parametrization in terms of some variable other than ω might have physical significance.

The question naturally arises whether the other structure function, W_1, also exhibits scaling behavior. A study of our results shows that, within errors, W_1 scales as a function of ω (or ω') over the same kinematic range as νW_2.

Figure 6 shows $2M_pW_1$ and νW_2 as functions of ω for $W\geq 2.6$ GeV, and Fig. 7 shows these quantities as functions of ω' for $W\geq 1.8$ GeV. The data presented in both figures are for $q^2>1$ (GeV/c)^2 and use $R=0.18$ in the evaluation of the points. The observed scaling behavior in ω and ω' is impressive for both structure functions over a large kinematic region.

Since W_1 and W_2 of Eq. (3) are related by

$$\frac{2M_pW_1}{\nu W_2}=\frac{\omega}{1+R}\left(1+\frac{2M_p}{\omega\nu}\right)=\frac{\omega'}{1+R}\left(1-\frac{a}{\omega' q^2}+\frac{2M_p}{\omega'\nu}\right), \tag{4}$$

it can be seen that scaling in W_1 accompanies scal-

ing in νW_2 only if R has the proper functional form to make the right-hand sides of the equations functions of ω (or ω'). In the Bjorken limit, it is evident that νW_2 and W_1 will mutually scale if R is a constant or a function of ω (or ω'). The measured values of R are small and are not sufficiently precise to determine its functional form.

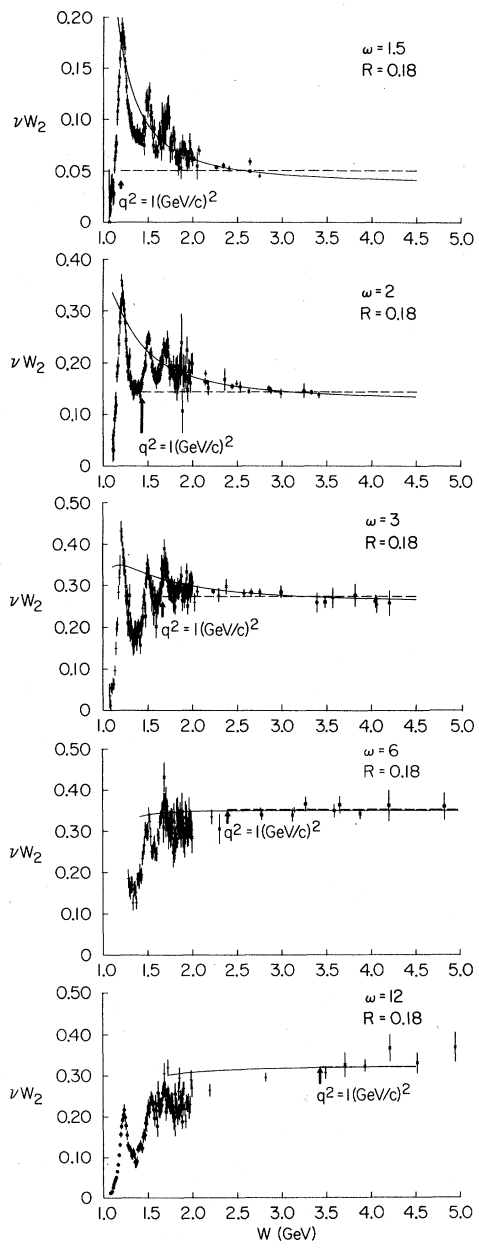

FIG. 5. Interpolated data are shown for five values of $\omega = 1.5$, 2, 3, 6, and 12. Scaling in ω would imply a constant value of νW_2 as W (or q^2) is varied. The curved solid line represents the fit to νW_2 as a function of ω' given in Eq. (6). Note that a graph with ω constant does not have ω' constant. The horizontal dashed line is the value of $F(\omega)$ from Eq. (5).

Parametric fits of νW_2 to the values shown in Figs. 6 and 7 give

$$\nu W_2 = F(\omega) = (1-1/\omega)^3[1.274+0.5989(1-1/\omega) - 1.675(1-1/\omega)^2] \quad (5)$$

and

$$\nu W_2 = F(\omega') = (1-1/\omega')^3[0.6453+1.902(1-1/\omega') - 2.343(1-1/\omega')^2]. \quad (6)$$

For either ω or ω' less than two, νW_2 can be satisfactorily fitted with a single cubic term, a result consistent with the threshold behavior of νW_2 predicted by models[14] which relate it to the elastic form factor. $2M_p W_1$ may be satisfactorily fitted by $(1-1/\omega')^3$ for $1.2 < \omega' < 1.5$ and by $(1-1/\omega')^4$ for $1.5 < \omega' < 5$.

The kinematic dependences of σ_T and σ_S give an intuitively different but equivalent picture of inelastic electron scattering from the proton. Figure 8 shows the cross sections σ_T and σ_S plotted for constant q^2 as functions of W^2. The dashed lines indicate the W^2 dependence of $\sigma_{\gamma p}$. For $q^2 \leq 3$ $(\mathrm{GeV}/c)^2$ the cross sections are consistent with a constant or a slowly falling energy dependence similar to the behavior of $\sigma_{\gamma p}$. For larger q^2, σ_T shows a rising energy dependence resembling a threshold-type behavior. This rising behavior of σ_T at high energy is unique among the various total cross sections that have been measured. The q^2 dependence of σ_T shown in Fig. 9 shows no pure power-law behavior but varies in the region of the present data between $1/q^2$ and $1/q^6$ as indicated by the straight lines shown in Fig. 9. The point $\omega' = 5$ roughly separates the threshold region of νW_2 from the flat, structureless region. The rising energy dependence of σ_T for large q^2 reflects the rising behavior of νW_2 for $\omega' < 5$. The $1/q^2$ dependence is correlated with the constancy of νW_2 for $\omega' > 5$, and the $1/q^6$ asymptotic dependence as ω' approaches unity corresponds to the asymptotic limit of the threshold behavior of νW_2 obtained using Eq. (6):

$$\lim_{q^2\to\infty;\ W^2=\text{const}} \nu W_2 = \frac{K}{4\pi^2\alpha}(\sigma_T+\sigma_S) \propto \lim_{q^2\to\infty;\ W^2=\text{const}} \left(\frac{1}{1+q^2/W^2}\right)^3 \propto \frac{1}{q^6}.$$

The results of our separation of σ_T and σ_S show that σ_T is dominant in the kinematic region that we have investigated. The smallness of R precludes a definite statement that σ_S is significantly different from zero. The lack of measurements in the region $2M_p\nu/q^2 > 10$ prohibits a comparison with some

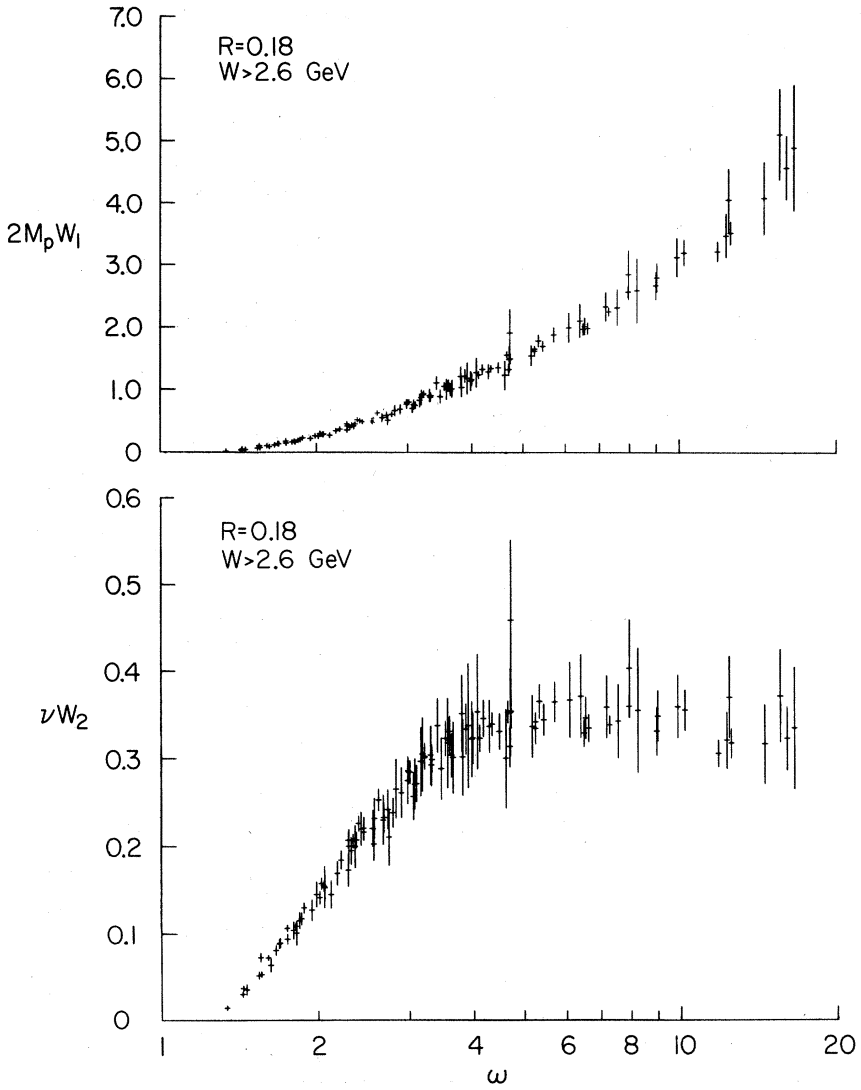

FIG. 6. $2M_pW_1$ and νW_2 are shown as functions of ω for $R = 0.18$, $W > 2.6$ GeV, and $q^2 > 1$ (GeV/c)^2.

diffractive models for R, but we find that R is small for values of $2M_p\nu/q^2$ up to about 8 and is not strongly varying with kinematics.

The new data permit further investigation of sum rules involving νW_2 reported with the 6° and 10° data.[10] Using $R = 0.18$, interpolations of both the small- and large-angle data were used to determine νW_2 at a constant value of $q^2 = 1.5$ (GeV/c)^2. The evaluation of the integral in the Gottfried sum rule,[15] based on a nonrelativistic pointlike quark model of the proton, gives

$$\int_1^{20} \frac{d\omega}{\omega} \nu W_2 = 0.78 \pm 0.04$$

when integrated over the range of our data.

We have also evaluated the Callan-Gross[16] sum rule, which is related to the equal-time commutator of the current and its time derivative and which is also equal to the mean square charge per parton in parton models.[17] For this integral we find

$$\int_1^{20} \frac{d\omega}{\omega^2} \nu W_2 = 0.172 \pm 0.009 ,$$

which is about one half the value predicted on the basis of a simple quark model of the proton, and is also too small for a proton described by a quark model with three "valence" quarks, in a sea of quark-antiquark pairs.

Recently, Bloom and Gilman[18] have proposed a constant-q^2, finite-energy sum rule based on scaling in ω' (Ref. 19) that equates an integral over νW_2 in the resonance region with the corresponding integral over the asymptotic expression for νW_2. They have pointed out that the applicability of the sum rule to spectra which have prominent resonances is indicative of a substantial nondiffractive component in νW_2. The sum rule requires that, at constant q^2, J_1 equal J_2 with

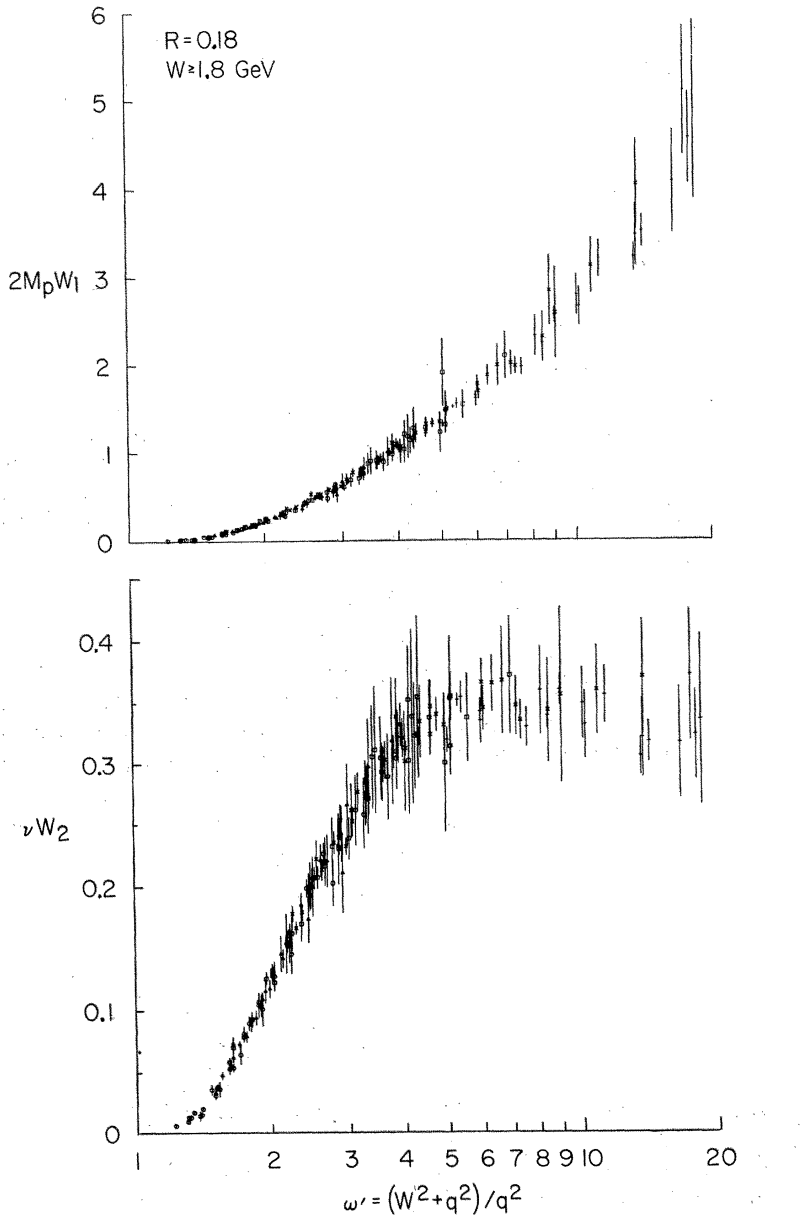

FIG. 7. $2M_pW_1$ and νW_2 are shown as functions of ω' for $R=0.18$, $W>1.80$ GeV, and $q^2>1$ (GeV/c)^2.

$$J_1 \equiv \left(\frac{2M_p}{q^2}\right)\int_0^{\nu_m} d\nu (\nu W_2)_{\text{exp}}$$

and

$$J_2 \equiv \left(\frac{2M_p}{q^2}\right)\int_0^{\nu_m} d\nu\, F(\omega') = \int_1^{\omega'_m} d\omega' F(\omega'),$$

where $(\nu W_2)_{\text{exp}}$ is given by interpolation, at fixed q^2, of the 6° and 10° data with $R=0.18$ and where $F(\omega')$ is given by Eq. (6). The upper limit is determined by choosing a missing mass W_m which is somewhat beyond the prominent resonance bumps, whence $2M_p\nu_m = W_m^2 - M_p^2 + q^2$. We find that in the range of q^2 from 1 to 4 (GeV/c)^2 and W_m from 2.2 to 2.5 GeV the maximum deviation of J_2 from J_1 is 9%. This result is only weakly sensitive to modest changes in R.

Parton models and diffraction models have been suggested to explain the inelastic scattering results. The scaling behavior observed in these measurements arises naturally in simple parton models in which the proton is made up of pointlike constituents, and, in general, diffraction models are not inconsistent with scaling. Preliminary analyses[12] of our recent measurements of inelastic electron-deuteron scattering suggest that there are differences between the inelastic electron-proton and electron-neutron cross sections. Such differ-

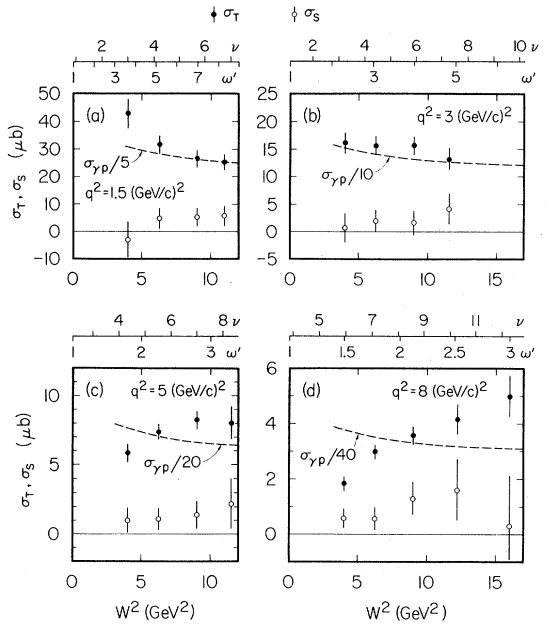

FIG. 8. The values of σ_T and σ_S given in Table III are shown at constant q^2 as a function of W^2 (or ν) for q^2 =1.5, 3, 5, and 8 (GeV/c)^2. Also shown is the ν dependence of the total photoabsorption cross section.

ences would point to a substantial nondiffractive component of the deep-inelastic cross section for values of ω less than approximately six.

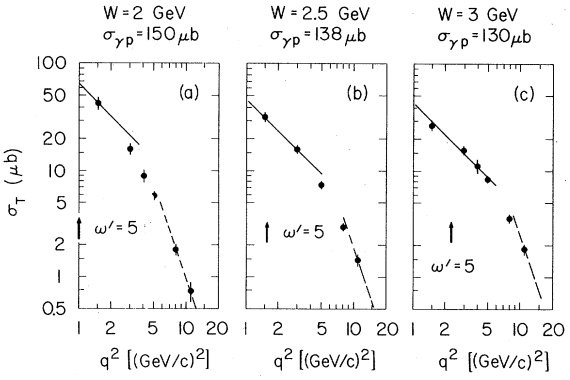

FIG. 9. The values of σ_T given in Table III are shown at constant W as a function of q^2 for W =2, 2.5, and 3.0 GeV. The solid line indicates a $1/q^2$ dependence and the dashed line represents a $1/q^6$ variation with q^2. The point ω' =5 is also indicated.

ACKNOWLEDGMENTS

The group wishes to thank Professor W. K. H. Panofsky, the Spectrometer Facilities Group, and the Technical Division under R. B. Neal for their support in this project.

The MIT collaborators are grateful for support extended them by the MIT Physics Department and the Laboratory for Nuclear Science during the program of experiments.

APPENDIX: RADIATIVE-CORRECTION FORMULAS

The measured cross section for the scattering of electrons of energy E from target protons into solid angle $d\Omega$ and energy dE' will be denoted by $d\sigma_{\rm rad}/d\Omega dE'$. The corrected cross section as defined here is the cross section calculated to lowest order in α, that is, assuming the exchange of a single photon with the lowest-order expressions for the photon propagator and electron-photon vertex used. The corrected cross section will be denoted by $d\sigma/d\Omega dE'$. This Appendix is based on the thesis of Miller[6] which includes discussions of the derivation of many of the formulas. Our treatment of multiple-photon corrections differs somewhat from that in Ref. 7.

A. General Formula

The formula used to radiatively correct the measured inelastic cross section was the following:

$$\frac{d\sigma}{d\Omega dE'}(E,E',\theta)=\left[\left(\frac{\Delta E}{E}\right)^{t/2+bt_b}\left(\frac{\Delta E'}{E'}\right)^{t/2+bt_a}\frac{1+\delta'(q^2)}{\Gamma(1+bt_b+bt_a)}\right]^{-1}$$

$$\times\left[\frac{d\sigma_{\rm rad}}{d\Omega dE'}(E,E',\theta)-\frac{d\sigma_{\rm elas\ rad}}{d\Omega dE'}(E,E',\theta)\right.$$

$$-\int_{E_{\rm min}}^{E-\Delta E}dE_1\left(\frac{v_b}{E-E_1}+t_b w(E,E_1)\right)\frac{d\sigma}{d\Omega dE'}(E_1,E',\theta)\left(\frac{k_1}{E}\right)^{t/2+bt_b}\left(\frac{k_1'}{E'}\right)^{t/2+bt_a}\frac{1+\delta'(q_1^2)}{\Gamma(1+bt_b+bt_a)}$$

$$\left.-\int_{E'+\Delta E'}^{E'_{\rm max}}dE_1'\left(\frac{v_a}{E_1'-E'}+t_a w(E_1',E')\right)\frac{d\sigma}{d\Omega dE'}(E,E_1',\theta)\left(\frac{k_1}{E}\right)^{t/2+bt_b}\left(\frac{k_1'}{E'}\right)^{t/2+bt_a}\frac{1+\delta'(q_1'^2)}{\Gamma(1+bt_b+bt_a)}\right].$$

(A1)

All quantities appearing in Eq. (A1) will be defined and discussed in this and the following sections of this Appendix. $d\sigma_{\text{elas rad}}/d\Omega dE'$ is the radiative tail from elastic e-p scattering. Its formula will be given in Sec. B of this Appendix.

The two integrals involve the corrected cross section and represent the radiative tails from inelastic production of higher-mass states of the proton. $E'_{\max}$ and $E_{\min}$ are the energies at pion threshold along the paths of integration:

$$\begin{aligned} E_{\min} &= (E' + m_\pi + m_\pi{}^2/2M_p)\eta', \\ E'_{\max} &= (E - m_\pi - m_\pi{}^2/2M_p)/\eta, \\ \Delta E &= \eta\eta'\Delta E', \end{aligned} \tag{A2}$$

where m_π is the pion mass, and M_p the proton mass. The kinematical quantities η and η' are given by

$$\begin{aligned} \eta &= 1 + \frac{2E}{M_p}\sin^2(\tfrac{1}{2}\theta), \\ \eta' &= \left[1 - \frac{2E'}{M_p}\sin^2(\tfrac{1}{2}\theta)\right]^{-1}. \end{aligned} \tag{A3}$$

It is an approximation that the inelastic radiative tail can be expressed only in terms of the corrected cross section at two points $(E-\omega, E', \theta)$ and $(E, E'+\omega', \theta)$ instead of as an integral involving the two inelastic form factors individually. (In this Appendix ω and ω' denote the energies of radiated photons defined by $\omega = E - E'\eta'$ and $\omega' = E/\eta - E'$, not the scaling variables defined earlier.) This so-called "peaking-factorization" approximation causes a maximum error of roughly 10% in the calculated radiative tail, which is tolerable in this case. v_b and v_a play the role of equivalent radiators for the hard-photon bremsstrahlung process.

The following equivalent radiators based on the peaking-factorization approximation were used. They were determined by inserting approximate inelastic form factors into formula (B.5) of Mo and Tsai.[7] These approximate form factors resulted from an analysis of the data using radiative corrections employing the standard equivalent-radiator description.

$$\begin{aligned} v_b &= \frac{t}{2}\left[\frac{E_1}{E} - 0.2\left(1 - \frac{E_1}{E}\right) + 0.7\left(1 - \frac{E_1}{E}\right)^2\right], \\ v_a &= \frac{t}{2}\left[\frac{E'}{E'_1} - 0.2\left(1 - \frac{E'}{E'_1}\right) + 0.7\left(1 - \frac{E'}{E'_1}\right)^2\right]. \end{aligned} \tag{A4}$$

The quantity t in the exponent of the soft-photon factor and in Eq. (A4) is given by

$$t = \frac{2\alpha}{\pi}\left(\ln\frac{q^2}{m^2} - 1\right), \tag{A5}$$

where m is the electron mass.

t_b and t_a are the thicknesses of material traversed by a detected electron, before and after the point of scattering, measured in radiation lengths. In practice the thickness of the liquid target is apportioned equally between t_b and t_a. In Eq. (A1), $b = \frac{4}{3} + a$, with a given by

$$\begin{aligned} a &= \frac{1}{9}\,\frac{Z+1}{Z+\zeta}\,\frac{1}{\ln(191\,Z^{-1/3}) - 1.2(\alpha Z)^2}, \\ \zeta &= \frac{\ln(1440\,Z^{-2/3})}{\ln(191\,Z^{-1/3}) - 1.2(\alpha Z)^2}. \end{aligned} \tag{A6}$$

$w(E, E_1)$ is the probability for an electron to lose energy $E - E_1$ by the emission of a single photon per unit radiation length of material; i.e.,

$$w(E, E_1) = \frac{1}{E - E_1}\left[1 + \left(\frac{E_1}{E}\right)^2 - \frac{E_1}{E}\left(\tfrac{2}{3} - a\right)\right]. \tag{A7}$$

Γ refers to the mathematical Γ function. $1 + \delta'$ is the radiative correction remaining after the $(\Delta E/E)^t$ soft-photon factor has been extracted. The quantity δ' is given by

$$\delta'(q^2) = \frac{2\alpha}{\pi}\left(\frac{13}{12}\ln\frac{q^2}{m^2} - \frac{14}{9}\right). \tag{A8}$$

The soft-photon limiting energies, k_1 and k'_1, are defined as follows:

$$\begin{aligned} k_1 &= \min(\tfrac{1}{3}E, \omega_1), \\ k'_1 &= \min(\tfrac{1}{3}E, \omega'_1). \end{aligned} \tag{A9}$$

The physical basis for these formulas is discussed in Sec. C of this Appendix. For the E integral, $\omega_1 = E - E_1$ and $\omega'_1 = \omega'/\eta\eta'$. For the E' integral, $\omega'_1 = E'_1 - E'$ and $\omega_1 = \eta\eta'\omega'$. The resulting corrected cross section must not be sensitive to the choice of the arbitrary factor $\frac{1}{3}$ in (A9) since this fraction is uncertain roughly within the range 0.2 to 0.8.

The q^2's in formula (A1) are defined as follows:

$$\begin{aligned} q^2 &= 4EE'\sin^2(\tfrac{1}{2}\theta), \\ q_1{}^2 &= 4E_1E'\sin^2(\tfrac{1}{2}\theta), \\ q'_1{}^2 &= 4EE'_1\sin^2(\tfrac{1}{2}\theta). \end{aligned} \tag{A10}$$

$\Delta E'$ is arbitrary as long as it is sufficiently small so that the cross section $d\sigma/d\Omega dE'$ does not vary appreciably over this range of energies. More precisely $d\sigma/d\Omega dE'$ is defined as the limit of the above expression (A1) for $\Delta E' \to 0$.

Assuming the cross section is measured only for a certain number of lines or spectra (E, θ const, E' varying), the corrected cross section must be interpolated and extrapolated from the measured lines in order to do the first integration in formula (A1). The precise relationship of the corrected cross section to the measured cross section is that the corrected cross section, when interpolated and extrapolated according to the scheme chosen,

satisfies Eq. (A1) along the measured lines. Our final results are insensitive to the method of interpolation used, but some of the results depend slightly on the method of extrapolation used.

B. Elastic Tail Correction

The formula used for the elastic radiative tail was the following:

$$\frac{d\sigma_{\text{elas}}}{d\Omega dE'}(E, E', \theta) = \left[\frac{d\sigma_1'}{d\Omega dE'}(E, E', \theta)\frac{t}{t_{\text{elas}}} + t_b w(E, E-\omega)\eta'^2 \frac{d\sigma_0'}{d\Omega}(E-\omega, \theta) + t_a w(E'+\omega', E')\frac{d\sigma_0'}{d\Omega}(E, \theta)\right]\frac{(k/\sqrt{EE'})^{t+bt_b+bt_a}}{\Gamma(1+bt_b+bt_a)}. \tag{A11}$$

$d\sigma_1'/d\Omega dE'$ is the cross section for bremsstrahlung during elastic scattering, calculated to lowest order in α, but including corrections to higher order in α to the photon propagator and electron-photon vertex. It is given by the formula (B.5) of Mo and Tsai,[7] with the modified proton elastic form factors F and G of (B.5), as follows:

$$F(q^2) = \frac{4[G_E^2(q^2) + (q^2/4M_p^2)G_M^2(q^2)]}{1+q^2/4M_p^2}[1+\delta'(q^2)],$$
$$G(q^2) = q^2 G_M^2(q^2)[1+\delta'(q^2)]. \tag{A12}$$

G_E and G_M were determined by a fit to elastic ep data, using the assumption of form-factor scaling: the relation $G_M(q^2) = 2.793\, G_E(q^2)$. The final results are insensitive to modest deviations from this relationship.

$d\sigma_0'/d\Omega$ is the corrected electron-proton elastic cross section given by the usual Rosenbluth formula, but with electrodynamic corrections,

$$\frac{d\sigma_0'}{d\Omega}(E, \theta) = \frac{\alpha^2}{4E^2}\frac{\cos^2(\tfrac{1}{2}\theta)}{\sin^4(\tfrac{1}{2}\theta)}\left[2M_p\frac{G_E^2(q^2) + (q^2/4M_p^2)G_M^2(q^2)}{1+q^2/4M_p^2} + 2\tan^2(\tfrac{1}{2}\theta)\frac{q^2}{2M_p}G_M^2(q^2)\right]\frac{1}{2M_p\eta}[1+\delta'(q^2)]. \tag{A13}$$

t_{elas} is the equivalent radiator associated just with the incoming and outgoing electrons,

$$t_{\text{elas}} = \frac{2\alpha}{\pi}\left(\ln\frac{q^2}{m^2} - 1\right). \tag{A14}$$

t is the total equivalent radiator, taking into account soft-photon radiation from the proton as well as from the electron and including electron-proton interference effects,[20]

$$t = t_{\text{elas}} + \frac{2\alpha}{\pi}\left(\frac{1+q^2/2M_p^2}{[(1+q^2/2M_p^2)^2-1]^{1/2}}\ln\{1+q^2/2M_p^2 + [(1+q^2/2M_p^2)^2-1]^{1/2}\} - 1\right) + \frac{4\alpha}{\pi}\ln\eta. \tag{A15}$$

Both t_{elas} and t are calculated at $(E-\omega, E', \theta)$ instead of (E, E', θ), where ω is the radiated energy, since this corresponds to the most probable momentum transfer to the proton and gives the q^2 which is most important in the large-angle bremsstrahlung process. The two terms in (A15) in addition to t_{elas} represent an attempt to estimate the effect of radiation coming from the proton including the interference term. k is an effective limiting soft-photon energy and is discussed in the following section.

C. Selection of the Limiting Soft-Photon Energy

If we neglect entirely all multiple hard-photon radiation we get the formula (A11) for the radiative tail from elastic scattering, $ep \to ep$. The quantity k is arbitrary, being the limiting soft-photon energy. In general, we expect that k should be a small fraction of E, E' in order for the soft-photon arguments to hold. As k goes to zero, the cross section given by (A11) also goes to zero, which means physically that soft-photon radiation always occurs.

The result (A11) depends on k, but the dependence is quite small. We expect that the correct radiative tail, including multiple hard-photon effects, can be put in the form (A11) with some value of k that is a fairly small fraction of the energies E and E'. A reasonable estimate for the actual radiative tail would be formula (A11) with $(k/E)^{t/2+bt_b}(k/E')^{t/2+bt_a}$ replaced by $(k/E)^{t/2+bt_b} \times (k'/E')^{t/2+bt_a}$, where

$$k = \min(\tfrac{1}{3}E, \omega), \quad k' = \min(\tfrac{1}{3}E', \omega'). \tag{A16}$$

The fraction $\frac{1}{3}$ is arbitrary and the variation of the

result with this fraction is a measure of our ignorance of the actual size of multiple hard-photon effects.

It is interesting to consider a model calculation that yields a specific value for k. We consider target energy losses only, that is, $t \ll t_b, t_a$. The radiative tail is then known exactly.

$$\frac{d\sigma}{d\Omega dE'} = \int \pi(E, E_1, t_b)\frac{d\sigma_0'}{d\Omega}(E_1, \theta)\pi(E_1', E', t_a)dE_1, \tag{A17}$$

using the known form of the straggling function $\pi(E, E', t)$ which is a solution of the well-known diffusion equation.[21] A good approximation for the straggling function is[6]

$$\pi(E, E_1, t) = w(E, E_1)t\left(\ln\frac{E}{E_1}\right)^{bt}\frac{1+btP(z)}{\Gamma(1+bt)}, \tag{A18}$$

where $z \equiv (E - E_1)/E$ and the correction form is a parametrization based on numerical solution of the diffusion equation[22] with the form

$$P(z) = 0.5388\,z - 2.1938\,z^2 + 0.9634\,z^3. \tag{A19}$$

A simpler and slightly different expression for $\pi(E, E_1, t)$ has been given recently by Tsai.[23] The effective soft-photon energy k is defined so that the result of formula (A11) agrees with the result of the integration (A17); i.e.,

$$\begin{aligned}\int \pi(E, E_1, t_b)\frac{d\sigma_0}{d\Omega}(E_1, \theta)\pi(E_1', E', t_a)dE_1 \\ = \left(\frac{k}{\sqrt{EE'}}\right)^{bt_b+bt_a}\frac{1}{\Gamma(1+bt_b+bt_a)} \\ \times\left[t_b w(E, E-\omega)\eta'^2\frac{d\sigma_0}{d\Omega}(E-\omega, \theta)\right. \\ \left. + t_a w(E'+\omega', E')\frac{d\sigma_0}{d\Omega}(E, \theta)\right].\end{aligned} \tag{A20}$$

Figure 10 shows $k/\sqrt{EE'}$ versus $\sqrt{\omega\omega'}/\sqrt{EE'}$ for several different conditions where for simplicity we have used $t_b = t_a$. The cross section is for elastic scattering, $ep \to ep$. The effective k is found to be insensitive to t_b and t_a. However, k depends on how rapidly the cross section varies. The graphs show k obtained when the cross section is given by the Rosenbluth formula with the usual dipole form factors, and also with the form factors taken to be $G_E(q^2) = 1$ and $G_M(q^2) = 2.793$.

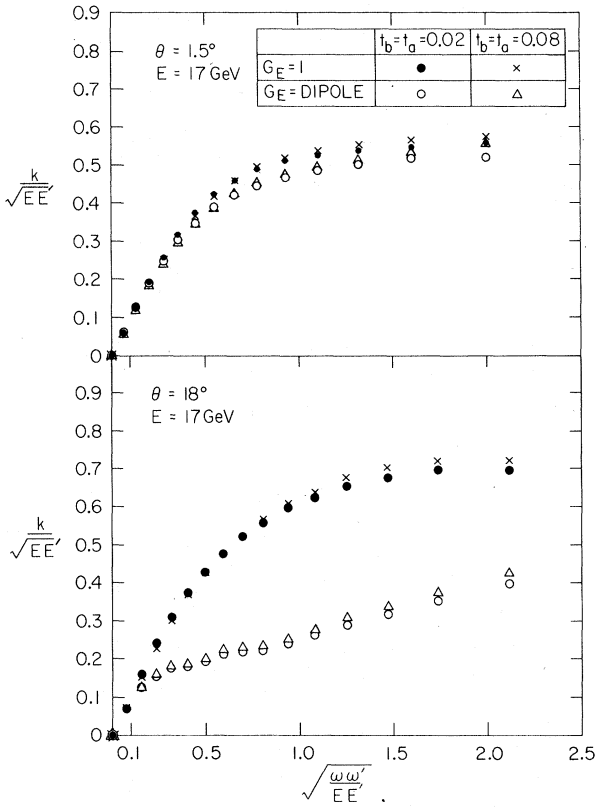

FIG. 10. The calculated limiting soft-photon energy k defined by Eq. (A 20) is shown for elastic scattering for two different kinematic conditions and two different assumptions about the q^2 variation of the form factors.

The above procedure was used for determining the value of k inserted into expression (A11) for calculating the radiative tail from the elastic peak, and is the basis for the formula (A16).

---

*Present address: Physics Department, University of Washington, Seattle, Wash. 98105.

†Present address: DESY, Hamburg, Germany.

‡Present address: Bonn University, Bonn, Germany.

§Present address: Department of Physics and Enrico Fermi Institute, University of Chicago, Chicago, Ill.

‖Work supported by the U. S. Atomic Energy Commission.

**Present address: Xerox Corporation, Rochester, N. Y.

††Work supported in part by the U. S. Atomic Energy Commission under Contract No. AT(30-1) 2098.

[1]E. D. Bloom *et al.*, Phys. Rev. Letters 23, 930 (1969).

[2]L. Hand, Ph.D. dissertation, Stanford University, 1961 (unpublished); Phys. Rev. 129, 1834 (1963).

[3]A detailed discussion of these quantities is given, for example, by F. Gilman, Phys. Rev. 167, 1365 (1968).

[4]P. N. Kirk *et al.* Phys. Rev. (to be published). An earlier and less complete discussion is given by R. E. Taylor, in *Proceedings of the Third International Symposium on Electron and Photon Interactions at High Energies, Stanford Linear Accelerator Center, Stan-*

ford, California, 1967 (Clearing House of Federal Scientific and Technical Information, Washington, D. C., 1968).

[5]R. Bell *et al.* IEEE Trans. Nucl. Sci. NS-16, 631 (1969).

[6]Guthrie Miller, Ph.D. dissertation, Stanford University, 1970 (unpublished), available as Stanford Linear Accelerator Center Report No. SLAC-129, 1971 (unpublished).

[7]L. W. Mo and Y. S. Tsai, Rev. Mod. Phys. 41, 205 (1969).

[8]D. H. Coward *et al.*, Phys. Rev. Letters 20, 292 (1969).

[9]The kinematic dependence $R=aq^2$, where a is a constant, is compatible with the gauge-invariance requirement that $\sigma_S=0$ at $q^2=0$. The relation $R=q^2/\nu^2$ would hold if, in the laboratory frame,

$$\sum_A |\langle A|j_{\parallel}^{\gamma}|p\rangle|^2=\sum_A |\langle A|j_{\perp}^{\gamma}|p\rangle|^2,$$

where p is the initial proton state, A is an arbitrary final state, $j_{\parallel}^{\gamma}$ and $j_{\perp}^{\gamma}$ are the longitudinal- and transverse-current operators, respectively, and the sum is over all possible final states. Such behavior leads to the relation between the structure functions, W_1 and W_2, $\nu W_2=(q^2/\nu)W_1$.

[10]M. Breidenbach, J. I. Friedman, H. W. Kendall, E. D. Bloom, D. H. Coward, H. DeStaebler, J. Drees, L. W. Mo, and R. E. Taylor, Phys. Rev. Letters 23, 935 (1969).

[11]J. D. Bjorken, Phys. Rev. 179, 1547 (1969).

[12]E. D. Bloom *et al.*, report presented to the Fifteenth International Conference on High Energy Physics, Kiev, U.S.S.R., 1970 [this report is available as SLAC Report No. SLAC-PUB-796 (unpublished)].

[13]Somewhat more discussion about ω' may be found in the dissertation of Miller, Ref. 6.

[14]S. Drell and T.-M. Yan, Phys. Rev. Letters 24, 181 (1970); G. B. West, *ibid.* 24, 1206 (1970).

[15]K. Gottfried, Phys. Rev. Letters 18, 1174 (1967).

[16]C. G. Callan, Jr. and D. J. Gross, Phys. Rev. Letters 21, 311 (1968).

[17]J. D. Bjorken and E. A. Paschos, Phys. Rev. 185, 1975 (1969). See also F. J. Gilman, in *International Symposium on Electron and Photon Interactions at High Energies, Liverpool, England, 1969,* edited by D. W. Braben and R. E. Rand (Daresbury Nuclear Physics Laboratory, Daresbury, Lancashire, England, 1970).

[18]E. D. Bloom and F. J. Gilman, Phys. Rev. Letters 25, 1140 (1970); also Phys. Rev. D 4, 2901 (1971).

[19]A family of finite-energy sum rules based on scaling in ω, relating the deep-inelastic and resonance regions, was proposed earlier by H. Leutwyler and J. Stern, Phys. Letters 31B, 458 (1970).

[20]In the general case of soft-photon radiation produced by an arbitrary number of particles, N, involved in a collision process, the average number of photons with energy in the range $d\omega$ is $d\bar{n}=t(d\omega/\omega)$, where t is given by

$$t=-\frac{\alpha}{\pi}\left[\sum_{\substack{j=1\\ j\neq i}}^{N}\sum_{i=1}^{N} Z_i Z_j \theta_i\theta_j \frac{a_{ij}}{b_{ij}} \ln\left(\frac{a_{ij}+b_{ij}+c_{ij}}{m_i^2+c_{ij}}\right)+N\right],$$

where particle i has charge eZ_i, four-momentum P_i (with $P_i\cdot P_j=\vec{P}_i\cdot\vec{P}_j-E_iE_j$), and direction of motion θ_i (+1 for incoming and −1 for outgoing), and where $a_{ij}=-(P_i\cdot P_j)$, $m_i^2=-(P_i\cdot P_i)$, $b_{ij}=[(P_i\cdot P_j)^2-m_i^2m_j^2]^{1/2}$, and $2c_{ij}=(m_i^4-m_i^2m_j^2)/(a_{ij}-m_i^2)$. Equation (A15) is the special case for elastic e-p scattering with the approximation that m^2 is negligible compared with M^2, E^2, and q^2.

[21]See, for example, B. Rossi, *High-Energy Particles* (Prentice-Hall, New York, 1952), Chap. V.

[22]R. Early, SLAC Group-A Internal Memorandum, 1969 (unpublished).

[23]Y. S. Tsai, lectures given at the NATO Advanced Institute on Electron Scattering and Nuclear Structure at Cagliari, Italy, 1970 [these lectures are available as SLAC Report No. SLAC-PUB-848 (unpublished)].